STRUCTURAL PHASE TRANSITION AND ELECTRODE CHARACTERISTICS OF $LiMn_{2-x}Mg_xO_4$ POSITIVE ELECTRODE MATERIAL FOR THE LITHIUM SECONDARY BATTERY

Yasushi Idemoto,[a] Kazuo Udagawa, [a] Nobuyuki Koura, [a]
James W. Richaradson, Jr.,[b] Ken Takeuchi, [b] and Chun -K.Loong[b]
[a] Department of Industrial Chemistry, Faculty of Science and Technology,
Science University of Tokyo, 2641 Yamazaki, Noda, Chiba 278-8510, JAPAN
[b] Intense Pulsed Neutron Source Division, Argonne National Laboratory,
Argonne, IL 60439-4814, USA

ABSTRACT

With in mind improving the cycle performance of 4V class lithium manganese oxide positive electrode material for the lithium secondary battery, we have been investigated the effects of partial substitution of Mn by another metal. The crystal phase transition in the quaternary spinel $LiMn_{2-x}Mg_xO_4$ was studied by neutron powder diffraction at 200K and DSC measurements at low temperatures. We find that substituting Mn by Mg resulted in a more stable crystal structure with the Jahn-Teller transition suppressed down to low temperature. The charge-discharge characteristics of these positive electrode active materials were investigated at 4V range. Although the discharge capacity decreased with increasing Mg content, the cycle performance was improved with increasing Mg content.

INTRODUCTION

The utilization of stoichiometric lithium manganese oxide as positive electrode material for the lithium secondary battery has been shown to exhibit poor cycling behavior. Yamada et al. reported a first-order Jahn-Teller structural phase transition of $LiMn_2O_4$ from cubic to tetragonal symmetry at around 280K (1). They also reported a suppression of the Jahn-Teller distortion by excess substitution of Mn with Li. Another approach to overcome these problems is to partially replace Mn by other transition metals, yielding $LiMn_{2-x}M_xO_4$(M = Co, Cr, Ni, Cu, Ti, Ge, Fe, Zn, Ga, Mg, V) (2)-(14), and $LiM_{\delta/2}Mn_{2-\delta}O_4$. (15). We have prepared a single-phase quaternary spinel $LiMn_{2-x}Mg_xO_4$ for x=0-0.2. The lattice parameter ***a*** decreases and the Mn valence increases with increasing Mg content. Partial substitution Mn with Mg improves the cycling performance in spite of some decrease of the initial capacity (16). The Jahn-Teller distortion is expected to occur at a temperature lower than that of $LiMn_2O_4$ because Mg^{2+} doping leads to a decrease of Mn^{3+} ions in the metal.

In this paper, we report the studies of the crystal phases and the electrochemical properties of $LiMn_{2x}Mg_xO_4$ by neutron powder diffraction, DSC measurements, and charge-discharge characterization.

DISCLAIMER

EXPERIMENTAL

Sample Preparation

$LiMn_{2-x}Mg_xO_4$ powders [x=0, 0.05, 0.10, 0.15, and 0.20] were prepared by reacting a appropriate mixture of $^7Li_2CO_3$ powder (99.99% purity and 99.9% ^7Li isotopic substitution, high Purity Chemical Ind. Ltd., Tomiyama), MnO_2 powder (99.5%, Wako Pure Chemical Ind. Ltd)., and MgO. (99.9%, Wako Pure Chemical Ind. Ltd.) Each mixture was preheated at 600 °C for 24h in air, then heated at 700 °C for 24h in oxygen.

Chemical Analysis

The $LiMn_{2-x}Mg_xO_4$ powders found to be single-phase materials by X-ray diffraction were subjected to chemical analysis.

A quantity of the sample was dissolved in a HCl solution and diluted with water. The total amount of Mn + Mg was determined with a standard solution of EDTA using BT as an indicator. The total amount of Mn was determined from the total amount of (Mn + Mg) and the Mn to Mg ratio obtained by the ICP method.

The average valence of the manganese ion was determined by iodometry and chemical analysis. A quantity of oxide sample was put in a saturated KI solution and hydrochloric acid was added and then stirred under Ar bubbling for the removal of dissolved oxygen.

The redox reactions that occurred are as follows:

$$[Mn^{4+}]_s + 4I^- \rightarrow MnI_2 + I_2 \quad [1]$$
$$[Mn^{3+}]_s + 3I^- \rightarrow MnI_2 + (1/2)I_2 \quad [2]$$
$$[Mn^{2+}]_s + 2I^- \rightarrow MnI_2 \quad [3]$$
$$[Mg^{2+}]_s + 2I^- \rightarrow MgI_2 \quad [4]$$

The total equivalent of $[Mn^{4+}]_s + [Mn^{3+}]_s$ was determined from the measured amount of liberated I_2 using a standard $Na_2S_2O_3$ solution. Consequently, their average valence was calculated from the amount of $[Mn^{4+}]_s + [Mn^{3+}]_s$ and the total amount of [Mn] ions.

Structural Analysis

The crystal phases and the lattice parameters of the powders at room temperature were first studied by X-ray diffraction (XRD) using a diffractometer with Cu-Kα radiation.

Time-of-flight neutron powder diffraction was performed using the General Purpose Powder Diffractometer (GPPD) at Argonne's Intense Pulsed Neutron Source (17). A powder sample of $Li(Mn_{2x}Mg_x)_2O_4$ [x=0, 0.2] was enclosed in a thin-wall vanadium can (11mm diameter, 50mm long). Independent TOF data were recorded on eight detector banks positioned at scattering angles ranging from ± 15° to ± 150°. The backscattering geometry (at a mean scattering angle of ±148°) corresponds to the highest resolution ($\Delta d/d$ = 0.25% where d is the atomic spacing). For each measurement, ~ 2.5 g of powder was used, and data were collected for 8h at 200K. The

crystal structure was refined with the Rietveld technique(GSAS program (18)), and these results were compared to the structure at room temperatures.

DSC Measurements

Differential scanning calorimetric (DSC) measurements were performed for the heating processes at a rate of 5K/min in the temperature range between 240Kand 330K. The samples, $LiMn_{2-x}Mg_xO_4$ (x = 0-0.2) were dried at 120°C for 1h in the argon before measurements. A sample was packed into a small aluminum cell designed for the apparatus (Rigaku Co., DSC-8230). The measurements were performed in a dry air atmosphere. The data were calibrated against those of an α-Al_2O_3 (99.999% purity) standard obtained under identical conditions.

Electrochemical Measurements

The electrochemical cell used was a three-electrode cell which employs a Li film (C. E. and R. E.) and a $LiMn_{2-x}Mg_xO_4$cathode (W. E., $10\times10mm^2$). The cathodes were prepared by pressing a blend of active material (30mg), acetylene black (10mg) and PTFE (10mg) onto a Ni mesh. The anodes were prepared by pressing a Li sheet onto a Ni mesh. The electrolyte used was 1M $LiClO_4$ in PC/DMC (1:1) solution. All procedures were carried out in an Ar-filled box.

Constant-current charge-discharge studies were controlled with a battery cycler (Hokuto Denkou, HJR-110mSM6). Cycling of the test materials was performed in sealed laboratory cells. Charge-discharge tests were performed at constant current density (0.2 mA cm^{-2}), with cutoff potentials of 3.5 to 4.3 V vs. Li/Li^+. The specific capacity was calculated from the value of the current, the mass of active material in the cathode, and the elapsed time.

RESULTS AND DISCUSSION

Sample Characterization

The X-ray diffraction profiles of the $LiMn_{2-x}Mg_xO_4$ (x = 0, 0.05, 0.1, 0.15, and 0.2) powders were identified as a single phase of cubic spinel (space group Fd3m). The x=0.3 sample was found to include a small amount of impurity (Li_2MnO_3). For $0 \leq x \leq 0.2$ the cubic lattice parameters obtained from XRD decrease with increasing Mg content (16). Based on this result, the boundary for a single-phase solid solution of $LiMn_{2-x}Mg_xO_4$ was estimated to be x=0.2. Hence, thorough measurements of other properties were made for the $LiMn_{2-x}Mg_xO_4$ ($x \leq 0.2$) sample.

The metal composition and the Mn valence of the $x \leq 0.2$ samples were determined by ICP and chemical analysis, respectively. These results were then used to evaluate the oxygen content according to the electroneutrality condition. We find that the Mn valence increases with increasing Mg content (16). We may also consider how Mg substitution affects the lithium storage capacity of $LiMn_2O_4$. The substitution of Mg^{2+} into the Mn-site is accompanied by an oxidation of Mn^{3+} to Mn^{4+} resulting in an increase in the average valency of the manganese ions, and thereby a suppression of the Jahn-Teller distortion. On the other hand, oxygen content was almost constant at about 4.04 below x=0.2.

Structural Analysis at Low Temperature

The neutron-diffraction intensity profiles of $LiMn_{2-x}Mg_xO_4$ [x=0 and 0.2] were analyzed over a wide range of d-spacing from 0.05 to 0.29nm. The samples were prepared by mixing $^7Li_2CO_3$ with MnO_2 and MgO so as to avoid the high neutron absorption of ^6Li. First, analysis of the $Li(Mn_{1-x}Mg_x)_2O_4$ [x=0 and 0.2] diffraction data at room temperature were carried out using an initial cubic structure (space group:Fd3m) with oxygen deficiency. Second, the 200K data were analyzed starting from a cubic (Fd3m) phase or orthorhombic (Fddd) phase with oxygen deficiency. The final refined parameters for $^7LiMn_2O_4$ at 200K are listed in Table 1. Figure 1 illustrates the result of the refinement of orthorhombic $^7LiMn_2O_4$ at 200K, where good agreement between observed and calculated patterns was obtained. In the case of $^7LiMn_{1.8}Mg_{0.2}O_4$ at 200K, on the other hand, a cubic structure was found, as shown in Table 2 and Figure 2.

From these results, we compared the goodness-fit indicator, $S=R_{wp}/R_e$. The S value for the orthorhombic $LiMn_2O_4$ is lower than that of cubic one. G. Rousse, et al. reported that stoichiometric spinel $LiMn_2O_4$ undergoes a transition from orthorhombic (observed at 230K) to a cubic symmetry (observed at 350K) by indexing the neutron diffraction patterns (19). Our results agree with Rousse's report. On the other hand, the S of cubic $LiMn_{1.8}Mg_{0.2}O_4$ is lower than that of orthorhombic one. From the results, $LiMn_2O_4$ is orthorhombic at 200K whereas $LiMn_{1.8}Mg_{0.2}O_4$ retains its room-temperature cubic phase down to 200K. Hence, the crystal structure is more stable at low temperature by the substitution of Mg for Mn.

DSC measurement

Figure 3 shows the DSC curves of $LiMn_{2-x}Mg_xO_4$ (x=0, 0.1, 0.15, and 0.2) for heating from 240K to 330K. The DSC curves of $LiMn_2O_4$ show a peak at ca. 270-280K, which corresponds to the phase transition caused by the Jahn-Teller effect. The peak intensity decreases with increasing Mg content in $LiMn_{2-x}Mg_xO_4$. We concluded from the results that the substitution of Mg for Mn suppressed the phase transition. The substitution of Mg^{2+} into the Mn-site is accompanied by a change of an oxidation of Mn^{3+} to Mn^{4+} resulting in an increase of the average valency of the manganese ions (16), and hence a suppression of the Jahn-Teller distortion.

Electrode Characteristics

The charge-discharge curves at the first cycle of the Li | $LiMn_{2-x}Mg_xO_4$ cell show that the initial discharge capacity was reduced by increasing the Mg content. From a previous paper (16), Mn valence increases with increasing Mg content. It suggests that even for the substituted spinel phases, only the Mn^{3+} ions contribute to the charge capacity, because the deintercalation of Li^+ from the l structure must be electronically compensated by the oxidation of Mn^{3+} to Mn^{4+}. Figure 4 shows the cycling performance in terms of discharge capacity obtained between 3.5 and 4.3V for $LiMn_{2-x}Mg_xO_4$ (x=0, 0.05, 0.1, 0.15, 0.2, and 0.3). The discharge capacity with respect to cycle number of the 4V region in the $LiMn_{2-x}Mg_xO_4$ electrodes shows a smaller diminishing rate with increasing Mg content, and Mg substitution results in improved cycle performance.

CONCLUSIONS

The relationship between the structural phase transition and electrode characteristics of the quaternary spinel $LiMn_{2-x}Mg_xO_4$ with respect to partial replacement of Mn by Mg was investigated. The Jahn-Teller transition was suppressed down to low temperature by the substitution of Mg for Mn, resulting in a more stable crystal structure. The effect of electrode characteristics for the positive electrode active materials was investigated over the 4V range. The discharge capacity decreased with increasing Mg content., however, the cycle performance was improved by increasing Mg content. It was concluded that the optimum composition is about $x = 0.1$ for $LiMn_{2-x}Mg_xO_4$.

ACKNOWLEDGEMENTS

This work has benefited from the use of the Intense Pulsed Neutron Source at Argonne National Laboratory. This facility is funded by the U.S. Department of Energy, Science, under the Contract W-31-109-Eng-38.

The authors wish to acknowledge H. Aoki and S. Ogawa for their experimental assistance.

REFERENCES

1. A. Yamada and M. Tanaka, *Mat. Res. Bull.*, **30**, 715 (1995).
2. Q. Zhong, A. Banakdarpour, M. Zhang, Y. Gao, and J. R. Dahn, *J. Electrochem. Soc.*, **144**, 205(1997).
3. L. Gouhara, H. Ikuta, T. Uchida, and M. Wakihara, *ibid.*, **143**, 178(1996).
4. Y. Ein-Eli and W. F. Howard,Jr., *ibid.*, **144**, L205 (1997).
5. J. M. Tarascon, E. Wang, F.K. Shokoohi, W.M. McKinnon, and S. Colson, *ibid.*,**138**, 2859(1991).
6. G. Pistoia, A. Antonini, R. Rosati, and C. Bellitto, *J. Electroanal. Chem.*, **410**, 115 (1996).
7. C. Sigala, D. Guyomard, A. Verbaere, Y. Piffard, and M. Tournoux, *J. Solid State Ionics*, **81**, 167(1995).
8. N. Kumagai, T. Fujiwara, and K. Tanno, *J. Electrochem. Soc.*, **140**, 3193(1993).
9. M. M. Thackeray, *ibid.*, **142**, 2558(1995).
10. A. D. Robertson, S. H. Lu, W. F. Averill, and W. F. Howard, Jr., *ibid.*, **144**, 3500 (1997).
11. D. Song, G. Li, H. Ikuta, and M.. Wakihara, *Denki Kagaku*, **66**, 1194(1998).
12. M. Yoshio, H. Noguchi, Y. Todorov, and Y. Hideshima, *Denki Kagaku*, **66**, 1198 (1998).
13. G. B. Appetecchi and B. Scrosati, *Denki Kagaku*, **66**, 1299(1998).
14. N. Hayashi, H. Ikuta, and M. Wakihara, *J. Electrochem. Soc.*, **146**, 1351(1999).
15. R. J. Gummow, A. de Kock, and M.M. Thackeray, *Solid State Ionics*, **69**, 59(1994).
16. Y. Idemoto, N. Koura,. and K. Udagawa, *Electrochemistry*, **67**, 235(1999).
17. J. D. Jorgensen, J. Faber,Jr., J. M. Carpenter, R.K. Crawford, J. R. Haumann, R. L. Hitterman, R. Kleb, G. E. Ostrowski, F. J. Rotella, .and T. G. Worlton, *J. Appl. Crystallogr.*, **22**, 321(1989).

18. A. C. Larson,.and R. B. von Dreele., *Los Alamos National Laboratory Report*, No. LA-UR 86-748 (1987).
19. G. Rousse, C. Masquelier, J. R. Caravajal, and M. Hervieu, *Electrochem. and Solid-State Lett.*, **2**, 6(1998).

Table 1 Crystal structural parameters for $^{7}LiMn_2O_4$ (oxygen defect model). Rietveld refinements were done in the cubic Fd3m space group (a) and the orthorhombic Fddd space group (b). The metal occupation factors were fixed.

(a) $^{7}LiMn_2O_4$ (Fd3m). R-factors are R_{WP} = 11.00 %, R_P = 7.80 % and R_{exp} = 6.36 %. $S=R_{wp}/R_e$=1.73

Atom	site	x	y	z	U_{11}(pm²)	U_{22}(pm²)	U_{33}(pm²)	U_{12}(pm²)	U_{13}(pm²)	U_{23}(pm²)	Site occupancy
Li	8a	0.125	0.125	0.125	217(21)	217(21)	217(21)	0.0	0.0	0.0	1.0
Mn	16d	0.5	0.5	0.5	126(8)	126(8)	126(8)	-26(6)	-26(6)	-26(6)	1.0
O	32e	0.26296(10)	0.26296(10)	0.26296(10)	136(5)	136(5)	136(5)	-21(4)	-21(4)	-21(4)	0.853(11)

lattice parameter : a = 8.2360(13) Å , V=557.77(3) Å^3

(b) $^{7}LiMn_2O_4$ (Fddd). R-factors are R_{WP} = 8.18 %, R_P = 5.85 % and R_{exp} = 6.36 %. $S=R_{wp}/R_e$=1.29

Atom	site	x	y	z	B_{iso}(Å²)	Site occupancy
Li	8a	0.125	0.125	0.125	1.24(10)	1.0
Mn	16d	0.5	0.5	0.5	0.89(4)	1.0
O	32e	0.26329(32)	0.26390(44)	0.26224(28)	1.06(3)	0.882(9)

lattice parameter : a=8.26254(33), b=8.23304(34), c=8.19870(28) Å , V=557.72(2) Å^3

Table 2 Crystal structural parameters for $^7LiMn_{1.8}Mg_{0.2}O_4$ (oxygen defect model) at 200K. Rietveld refinements were done in the cubic Fd3m space group (a) and the orthorhombic Fddd space group (b). The metal occupation factors were fixed.

(a) $^7LiMn_{1.8}Mg_{0.2}O_4$ (Fd3m). R-factors are R_{WP} = 7.25 %, R_p = 5.16 % and R_{exp} = 5.81 %. $S=R_{WP}/R_e$=1.25

Atom	site	x	y	z	U_{11}(pm²)	U_{22}(pm²)	U_{33}(pm²)	U_{12}(pm²)	U_{13}(pm²)	U_{23}(pm²)	Site occupancy
Li	8a	0.125	0.125	0.125	214(13)	214(13)	214(13)	0.0	0.0	0.0	1.0
Mn	16d	0.5	0.5	0.5	98(5)	98(5)	98(5)	-12(4)	-12(4)	-12(4)	0.9
Mg	16d	0.5	0.5	0.5	95(5)	95(5)	95(5)	-12(4)	-12(4)	-12(4)	0.1
O	32e	0.26306(5)	0.26306(5)	0.26306(5)	121(3)	121(3)	121(3)	-23(2)	-23(2)	-23(2)	0.879(8)

lattice parameter : a = 8.20984(7) Å , V=553.355(13) Å³

(b) $^7LiMn_{1.8}Mg_{0.2}O_4$ (Fddd). R-factors are R_{WP} = 7.87 %, R_p = 5.81 % and R_{exp} = 5.81 %. $S=R_{wp}/R_e$=1.35

Atom	site	x	y	z	B_{iso}(Å²)	Site occupancy
Li	8a	0.125	0.1250.5	0.125	1.53(9)	1.0
Mn	16d	0.5	0.5	0.5	0.79(4)	0.9
Mg	16d	0.5	0.5	0.5	0.79(4)	0.1
O	32e	0.26374(49)	0.26271(74)	0.26310(37)	1.07(2)	0.881(9)

lattice parameter : a = 8.22465(32), b=8.21137(35), c=8.19337(24) Å , V=553.34(1) Å³

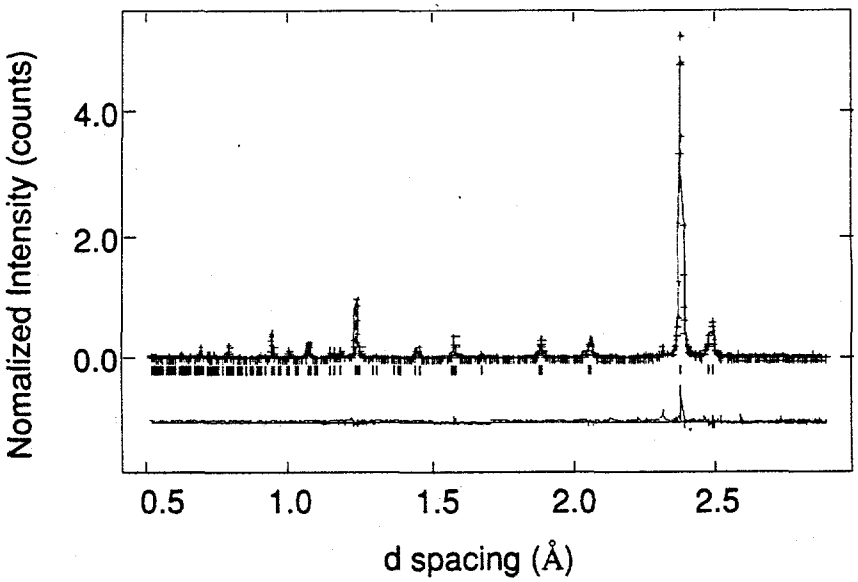

Fig. 1 Neutron powder diffraction data and Rietveld refinement profile fit for orthorhombic $^7LiMn_2O_4$ in the oxygen defect model at 200K. The plus marks are raw time-of-flight neutron powder diffraction data. The solid line is the calculated profile. Tick marks below the diffraction profile mark the positions of allowed Bragg reflections. The differences between the observed and calculated intensities are shown at the bottom. The background was fitted as part of the refinement but has been subtracted prior to plotting.

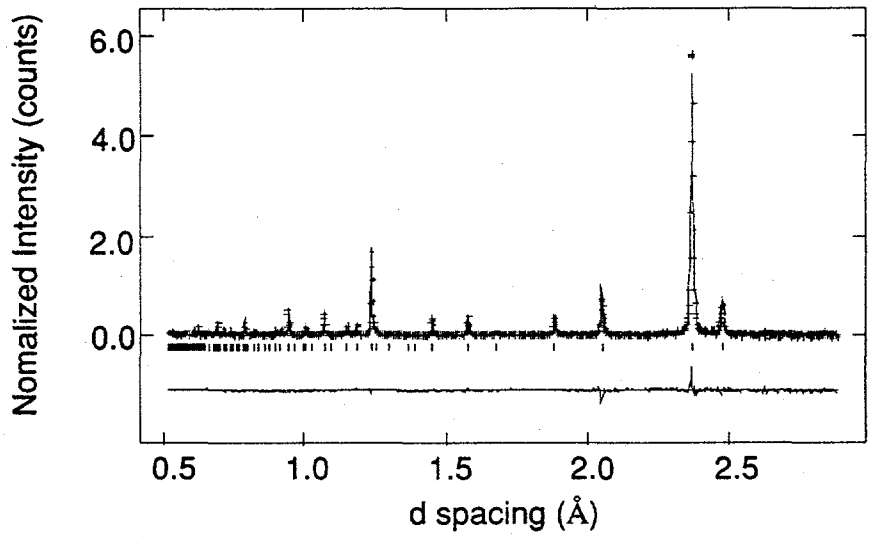

Fig. 2 Neutron powder diffraction data and Rietveld refinement profile fit for cubic $^7LiMn_{1.8}Mg_{0.2}O_4$ in the oxygen defect model at 200K. The plus marks are raw time-of-flight neutron powder diffraction data. The solid line is the calculated profile. Tick marks below the diffraction profile mark the positions of allowed Bragg reflections. The differences between the observed and calculated intensities are shown at the bottom. The background was fitted as part of the refinement but has been subtracted prior to plotting.

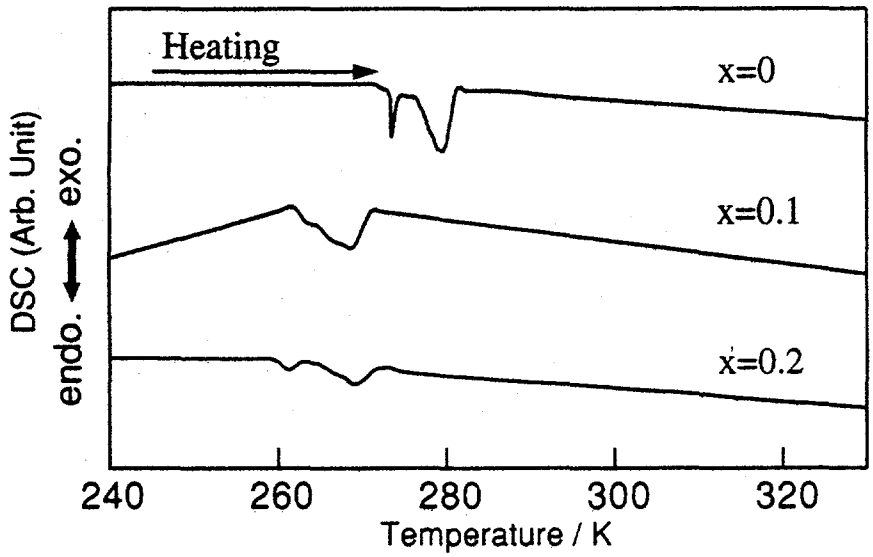

Fig. 3 DSC curves of $LiMn_{2-x}Mg_xO_4$ (x=0, 0.1, 0.2) measured in the temperature range between 240 K and 330 K for heating processes.
Heating rate : 5K/min, Atomosphere : Air

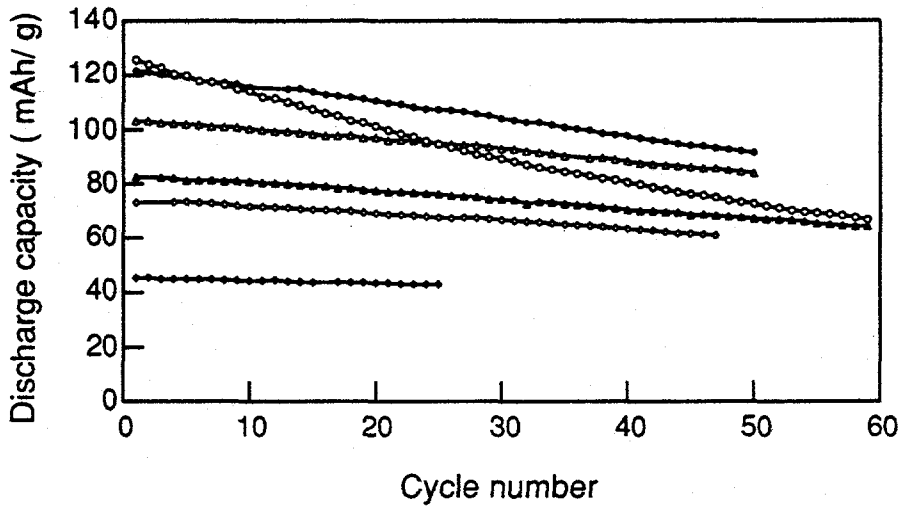

Fig. 4 Relation between discharge capacity and cycle number of $LiMn_{2-x}Mg_xO_4$.
(○:x=0, ●:x=0.05, △:x=0.1, ▲:x=0.15, ◇:x=0.2, ◆:x=0.3)
C.D.:0.2mA cm^{-2}, Cut-off voltage:4.3-3.5 V, 25℃.